

Proteomics-based evaluation of AAV dystrophin gene therapy outcomes in *mdx* skeletal muscle

Erynn E. Johnson,¹ Theodore R. Reyes,^{2,3} Jeffrey S. Chamberlain,^{2,3,4} James M. Ervasti,¹ and Hichem Tasfaout^{2,3}

¹Department of Biochemistry, Molecular Biology and Biophysics, University of Minnesota - Twin Cities, Minneapolis, Minnesota, USA. ²Department of Neurology, ³Senator Paul D. Wellstone Muscular Dystrophy Specialized Research Center, and ⁴Department of Biochemistry, University of Washington School of Medicine, Seattle, Washington, USA.

Duchenne muscular dystrophy (DMD) is a fatal genetic muscle-wasting disease characterized by loss of dystrophin protein. Therapeutic attempts to restore a functional copy of dystrophin to striated muscle are under active development, and many utilize adeno-associated viral (AAV) vectors. However, the limited cargo capacity of AAVs precludes delivery of full-length dystrophin, a 427 kDa protein, to target tissues. Recently, we developed a method to express large dystrophin constructs using the protein *trans*-splicing mechanism mediated by split inteins and myotropic AAV vectors. The efficacy of this approach to restore muscle function in *mdx*^{4cv} mice was previously assessed using histology, dystrophin immunolabeling, and Western blotting. Here, we expand our molecular characterization of dystrophin constructs with variable lengths using a mass spectrometry-based proteomics approach, providing insight into unique protein expression profiles in skeletal muscles of wild-type, dystrophic *mdx*^{4cv}, and AAV-treated *mdx*^{4cv} mice. Our data reveal several affected cellular processes in *mdx*^{4cv} skeletal muscles with changes in the expression profiles of key proteins to muscle homeostasis, whereas successful expression of dystrophin constructs results in an intermediate to complete restoration. This study highlights several biomarkers that could be used in future preclinical or clinical studies to evaluate the effectiveness of therapeutic strategies.

Introduction

Duchenne muscular dystrophy (DMD) is an inherited, lethal X-linked muscle-wasting disease. Affected patients typically show the first symptoms at approximately 3 years of age (1). The muscle function deteriorates rapidly starting at the age of 7 years with pronounced muscle weakness, chronic inflammation, and fibrosis, leading to loss of ambulation and premature death in the second to the third decade of life due to cardiorespiratory complications. DMD is caused by loss-of-function mutations in the *DMD* gene that abolish the production of a functional dystrophin (2–4). In muscle, dystrophin constitutes a key partner to several proteins, which together form the dystrophin-glycoprotein complex (DGC) (5). This complex plays an important role in preserving myofiber integrity during muscle contraction by connecting the intracellular cytoskeleton to the extracellular matrix (ECM) and serves as a molecular anchor to proteins involved in cellular signaling pathways regulating myofiber homeostasis (6).

Since DMD is a monogenic disease, restoring muscle function by supplying a functional copy of a dystrophin gene is a highly appealing therapeutic strategy. Several preclinical and clinical programs are in development to evaluate the efficacy and safety of systemic delivery of adeno-associated viral (AAV) vectors carrying dystrophin-based constructs to striated muscles (7). These vectors have been successfully used to express transgenes in a variety of organs, such as the liver, brain, retina, and muscles, and have shown a robust and long-term expression of transgenes with superior efficacy compared with other viral or non-viral vectors. However, AAV particles are relatively small (~20 nm) and, thus, present a limited packaging capacity to sequences of less than 5 kb (8), which poses an enormous challenge to genetic disorders with larger proteins like DMD. Dystrophin muscle isoform (Dp427) is expressed from an 11.2 kb cDNA, which far exceeds the AAV maximal packaging capacity.

Conflict of interest: HT and JSC are inventors on international patent application WO2023004125A2 describing the use of the split intein technology to express large proteins in muscular disorders, which was licensed by KineaBio. HT and JSC serve as scientific advisors to KineaBio.

Copyright: © 2025, Johnson et al. This is an open access article published under the terms of the Creative Commons Attribution 4.0 International License.

Submitted: July 8, 2025

Accepted: November 25, 2025

Published: November 27, 2025

Reference information: *JCI Insight*. 2026;11(2):e197759.
<https://doi.org/10.1172/jci.insight.197759>.

Therefore, tremendous efforts have been made over the last decades to study the structural organization of dystrophin, which later led to the development of a new class of dystrophin-based gene therapies. Early studies have shown that large in-frame deletions (up to 46%) within the central rod domain result in the production of a mini-dystrophin that retains functionality and protects striated muscle from mechanical damage (9). Additional phenotypical characterizations of transgenic mice demonstrate the efficacy of these mid-size dystrophins and shed light on the modular organization of dystrophin (10–12). These studies also showed that truncated dystrophins, termed micro-dystrophins (μ Dys), that fit within the AAV cargo capacity are stable and functional. The administration of AAV- μ Dys vectors into DMD animal models resulted in significant correction of muscular dystrophy (13–16). Several μ Dys constructs are being evaluated in the clinic, with one drug already approved by the FDA (Elevidys). Nonetheless, an increasing number of pre-clinical and clinical data point to incomplete muscle recovery with various μ Dys constructs. This suggests the need to express larger dystrophins to fully restore the functional impairment.

Recently, we described a method for delivering and expressing large dystrophins using protein *trans*-splicing (PTS) mediated by split inteins and myotropic AAV vectors (17). PTS is a natural phenomenon originally discovered in unicellular organisms by which 2 protein halves are seamlessly fused into a functional protein (18). We adapted this posttranscriptional process to express a large midi-dystrophin (midi-Dys, Δ SR5–15) or full-length dystrophin (full-Dys) (Dp427 isoform) using, respectively, a dual or triple AAV approach (17, 19). With this method, efficient reconstitution of large dystrophin was achieved using low doses of AAVMYO1 ($2\text{--}4 \times 10^{13}$ vg/kg) in both young (mildly affected) or old (severely affected) *mdx*^{Acv} mice, which restored several functional defects to normal levels. Nonetheless, the molecular characterization of the phenotypical rescue was limited to histology assessment using common staining methods, immunolabeling of dystrophin and its glycoprotein partners, or Western blotting. Although valuable to determine the protein expression and distribution, as well as the general muscle morphology, alternative methods that give deeper insight into specific defects or protein regulation may identify biomarkers that better delineate the stages of disease progression and serve as outcome measures in clinical trials conducted using AAV-dystrophin approaches.

Here, we describe a sensitive mass spectrometry-based (MS-based) proteomics workflow that allows a holistic analysis of protein expression of wild-type (WT), saline-, or AAV-treated *mdx*^{Acv} mice. Our data revealed subtle changes in dystrophic muscles expressing different dystrophin-based constructs and led to the identification of cellular biomarkers with variable expression profiles.

Results

Validation of dystrophin gene therapy replacement. We employed an isobaric labeling multiplex discovery proteomics approach to compare the skeletal muscle proteomes of healthy (WT), dystrophic (*mdx*^{Acv}), and AAVMYO1-treated *mdx*^{Acv} mice with variable dystrophin constructs. Myotropic AAVMYO1 vectors were administered systemically into 8-week-old mice at low doses of 2×10^{13} vg/kg to express μ Dys5 (Δ SR2–15, Δ 18–21, Δ CT) from a single vector or midi-Dys (Δ SR5–15) from dual vector, whereas triple AAVMYO1 were mixed and injected at a total dose of 4×10^{13} vg/kg to express full-Dys (Figure 1, A–C). Three months later, gastrocnemius muscles were collected from 6 AAV-treated mice as well as age-matched saline-treated *mdx*^{Acv} and WT mice. Protein lysates were extracted and labeled with TMT isobaric tags, and 2 proteomics screens were conducted (Figure 1D).

To verify dystrophin expression in each experimental group, construct-specific dystrophin peptide abundances were assessed (Table 1). Transgenic dystrophin constructs were detected in the samples from *mdx*^{Acv} mice treated with single, dual, or triple AAVs, but at lower abundance versus endogenous dystrophin in WT muscles (Figure 2A). As expected, the average abundance of peptide sequences specific to full-Dys was found elevated exclusively in WT or triple-AAV groups (Figure 2B). Similarly, peptide sequences specific to transgenic/human dystrophins (μ Dys5, intein-generated midi-Dys, or full-Dys) were elevated across all AAV treatment groups (Figure 2C). Using different peptides, μ Dys and midi-Dys were detected at comparable levels, whereas average full-Dys abundance was slightly lower. Finally, by searching peptides specific to large dystrophin (i.e., excluding μ Dys), we confirmed the exclusive expression of large dystrophins in WT or *mdx*^{Acv} mice treated with dual or triple AAV vectors (Figure 2D). Overall, the abundance of the dystrophins was peptide dependent, with a variable sensitivity observed from one peptide to another.

Together, these data highlight the specificity of this approach to detecting and quantifying endogenous or ectopic dystrophin proteins using specific sequences in healthy or dystrophic muscles after AAV treatment with different gene replacement approaches.

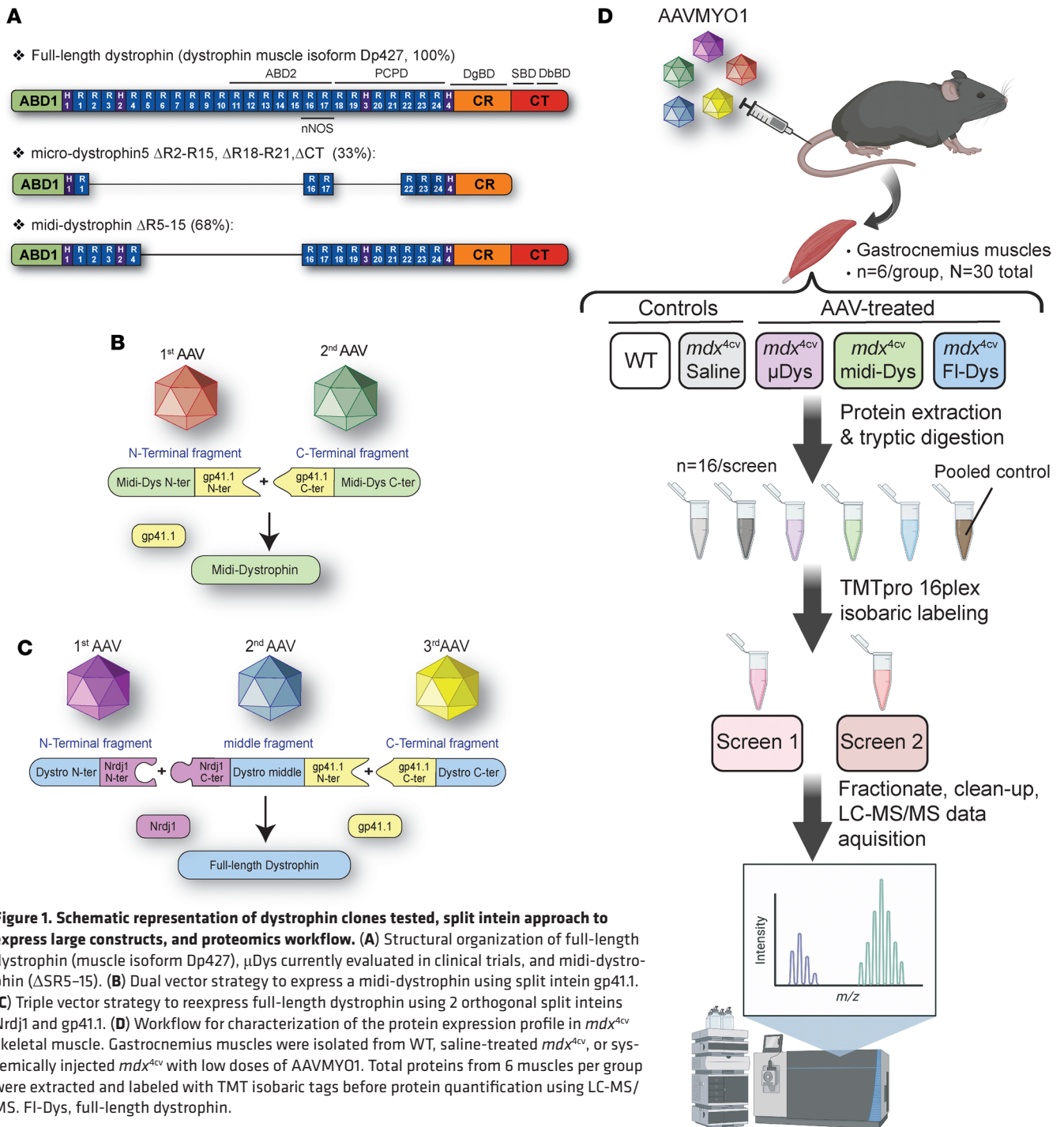


Figure 1. Schematic representation of dystrophin clones tested, split intein approach to express large constructs, and proteomics workflow. (A) Structural organization of full-length dystrophin (muscle isoform Dp427), μ Dys currently evaluated in clinical trials, and midi-dystrophin ($\Delta R5-15$). (B) Dual vector strategy to express a midi-dystrophin using split intein gp41.1. (C) Triple vector strategy to reexpress full-length dystrophin using 2 orthogonal split inteins Nrdj1 and gp41.1. (D) Workflow for characterization of the protein expression profile in mdx^{4cv} skeletal muscle. Gastrocnemius muscles were isolated from WT, saline-treated mdx^{4cv} , or systemically injected mdx^{4cv} with low doses of AAVMYO1. Total proteins from 6 muscles per group were extracted and labeled with TMT isobaric tags before protein quantification using LC-MS/MS. FI-Dys, full-length dystrophin.

Muscle histology improvement after dystrophin expression. To evaluate the muscle histology and compare the therapeutic benefits of each gene replacement modality, serial cross sections of gastrocnemius were stained with hematoxylin and eosin (H&E), trichrome, or immunolabeled using specific antibodies raised against elements of the DGC or periostin. In the group treated with AAVs, dystrophin expression was detected in 40%–60% of myofibers, whereas a few revertant fibers, not exceeding 1%, were found in the saline group (Figure 3, A and B). As gastrocnemius muscles are predominantly composed of fast-twitch myofiber type II, more than 86% of dystrophin-positive fibers were either type IIa, IIb, or IIx (Supplemental Figure 1; supplemental material available online with this article; <https://doi.org/10.1172/jci.insight.197759DS1>). Muscles from animals treated with saline presented typical dystrophic muscle histology with small fibers

Table 1. Dystrophin peptide sequences used in spectrum matching and quantifying endogenous murine full-length dystrophin (WT dystrophin) or transgenic/human dystrophin constructs delivered by AAVMYO1 vectors (μ Dys5, midi-Dys, and full-Dys constructs)

Peptide ID	Peptide Sequence	Location (encoding exon)	Data represented in
Peptide sequences specific to full-length dystrophin (WT dystrophin and full-Dys construct)			
Peptide F1	ELHEEAVR	Spectrin repeat 9 (exons 29–30)	Figure 2B
Peptide F2	VLSQIDVAQK	Spectrin repeat 10 (exons 31–32)	
Peptide F3	SEVEMVIK	Spectrin repeat 11 (exon 33)	
Peptide F4	ETLVEDK	Spectrin repeat 12 (exon 35)	
Peptide F5	QQLLQTK	Spectrin repeat 14 (exon 39)	
Peptide sequences specific to transgenic/human dystrophins (shared between μ Dys5, midi-Dys, and full-Dys constructs)			
Peptide hD1	WYNAQFSK	Calponin-homology (CH) 1 (exon 2)	Figure 2C
Peptide hD2	YQLGIEK	Calponin-homology (CH) 2 (exon 7)	
Peptide hD3	LLDPEDVDTTYPDKK	Calponin-homology (CH) 2 (exon 7–8)	
Peptide hD4	VGNILQLGSK	Spectrin repeat 1 (exon 11)	
Peptide hD5	TAALQSATPVER	Spectrin repeat 16 (exon 43)	
Peptide hD6	TDASILQEK	Spectrin repeat 17 (exon 45)	
Peptide hD7	QAEEVNTEWEK	Spectrin repeat 23 (exon 59)	
Peptide hD8	LNLHSADWQR	Spectrin repeat 23 (exon 59)	
Dystrophin peptide sequences specific to large dystrophins (shared between WT dystrophin, midi-Dys, and full-Dys constructs)			
Peptide L1	VLMDLQNQK	Spectrin repeat 2 (exon 12)	Figure 2D
Peptide L2	VLQEDLEQEQVR	Spectrin repeat 2 (exon 13)	
Peptide L3	QASEQLNSR	Spectrin repeat 4 (exon 20)	
Peptide L4	QTNLQWIK	Spectrin repeat 18 (exon 47)	
Peptide L5	DSTQWLEAK	Spectrin repeat 21 (exon 53)	
Peptide L6	DYSADDTR	Spectrin repeat 21 (exon 54)	
Peptide L7	SHLEASSDQWKR	Spectrin repeat 22–23 (exon 57)	
Peptide L8	ILADLEEENR	Carboxy-terminal domain (exons 74–75)	
Peptide L9	DAELIAEAK	Carboxy-terminal domain (exon 75)	
Peptide L10	QLESQLHR	Carboxy-terminal domain (exon 75)	
Peptide L11	QLLEQPQAEAK	Carboxy-terminal domain (exons 75–76)	

Mismatched residues of human versus murine sequences are underlined.

and fibrotic and infiltrated muscle tissue compared with WT muscles (Figure 3, A, and C–E). In contrast, muscle from mdx^{Acv} mice treated with AAVs showed improved histology with a substantial increase in myofiber area and diameter, with the highest values observed with large dystrophins (i.e., midi- and full-Dys). A marked reduction in collagen content was also found in groups treated with AAVs (Figure 3, A and C). Similarly, immunolabeling of periostin showed an increased area in saline-treated dystrophic muscles, confirming the expansion of the ECM, which AAV-dystrophin treatment prevented (Figure 3F). Interestingly, while proteomics data confirmed the upregulation of periostin (Figure 3G), variable abundance of collagen isoforms was observed. For instance, collagen isoform I ($\alpha 1$ and $\alpha 2$), IV ($\alpha 1$ and $\alpha 2$), VI ($\alpha 1$, $\alpha 2$, and $\alpha 3$), and XII abundance was unchanged among groups, whereas collagen type III ($\alpha 1$), V ($\alpha 2$ and $\alpha 3$), VI ($\alpha 6$), and XIV ($\alpha 1$ chain) abundance was elevated in mdx^{Acv} muscle and restored by AAV treatment (Figure 3H and Supplemental Figure 2).

Characterization of molecular changes using proteomics. Next, we investigated general trends in protein expression profiles between WT, mdx^{Acv} , and AAV treatment groups. Dystrophin-deficient mdx^{Acv} gastrocnemius muscle displayed a large number of differentially expressed proteins (DEPs) compared with WT muscle, including 250 upregulated proteins and 31 downregulated proteins (Figure 4A). The top upregulated and downregulated pathways in mdx^{Acv} muscle have been previously reported in mdx mice, demonstrating defects in, for example, cytoskeletal structure and sarcolemmal integrity (6, 20), ECM organization (21–23), and fatty acid metabolism (24, 25).

In contrast, few proteins displayed significantly elevated or depleted levels in single, dual, or triple AAV-treated mdx^{Acv} gastrocnemius muscle compared with WT muscle (Figure 4, B–D). A total of 16 upregulated and 3 downregulated proteins were identified between μ Dys5- mdx^{Acv} and WT mice (Figure 4B). Eighteen upregulated proteins and 5 downregulated proteins were observed in midi-Dys- mdx^{Acv} muscle

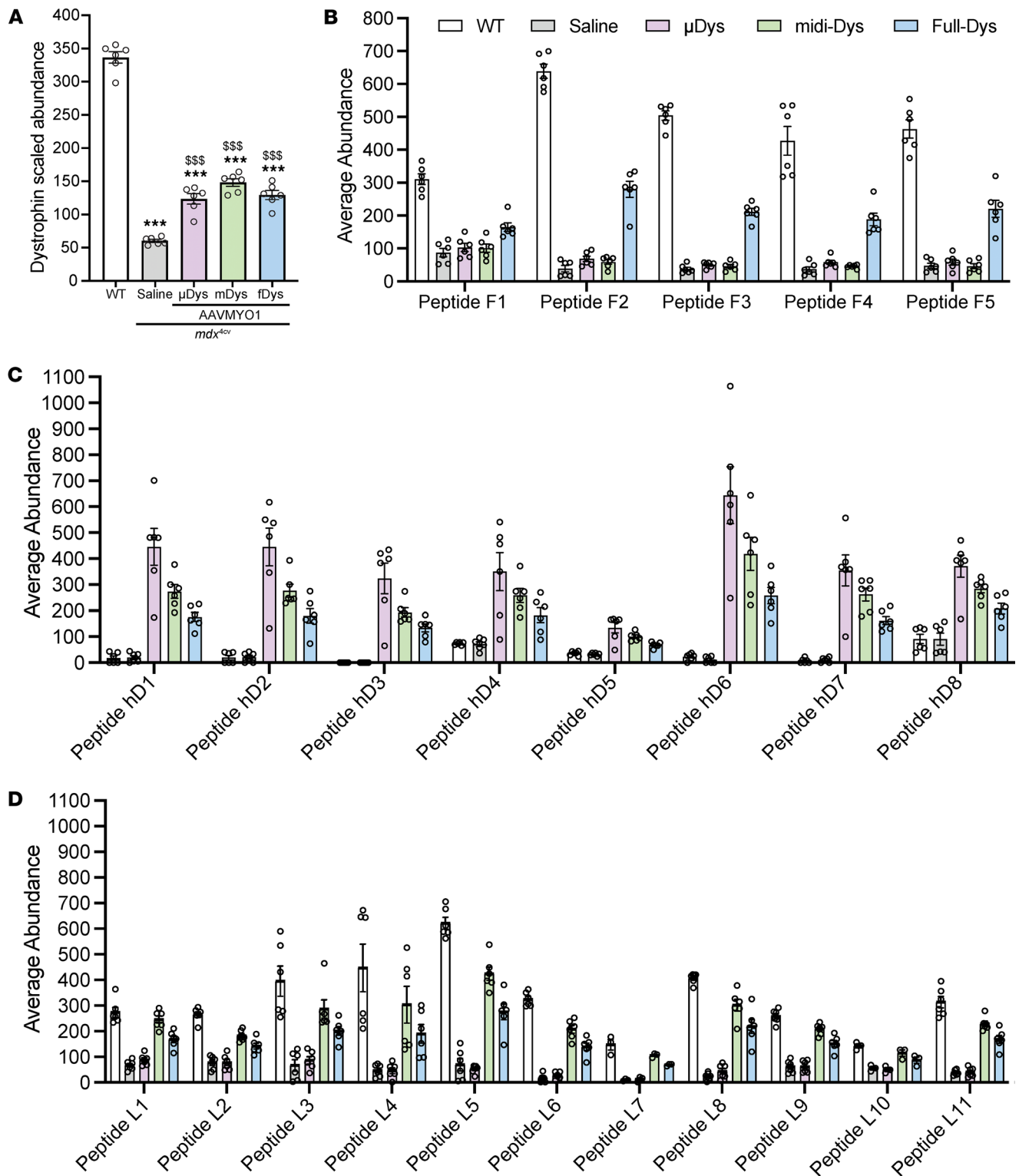


Figure 2. Detection of dystrophin expression and quantification of peptide-specific abundance using proteomics. Dystrophin peptide abundances were quantified using TMT proteomics in gastrocnemius muscle samples of WT, *mdx^{4cv}* treated with saline or AAVMYO1 to express μ Dys-*mdx^{4cv}*, midiDys-*mdx^{4cv}*, and full-Dys-*mdx^{4cv}*. **(A)** Quantified abundance of AAV-mediated dystrophin expressed in *mdx^{4cv}* mice versus endogenous full-Dys in WT mice. **(B)** Abundance of peptides present only in full-Dys (endogenous dystrophin in WT and full-Dys construct via triple AAVMYO1 treatment). **(C)** Abundance of peptides specific to transgenic/human dystrophins (shared between μ Dys5, midi-Dys, and full-Dys constructs) delivered by AAVMYO1. **(D)** Abundance of peptides specific to large dystrophins (endogenous WT dystrophin, or AAV-delivered midi-Dys and full-Dys constructs). The non-zero value for dystrophin peptides in saline-treated *mdx^{4cv}* is most likely due to coisolation interference common to TMT proteomics analyses. Bar graphs depict mean \pm SEM of $n = 6$ mice/group, except peptide L7 and L10, which were $n = 3$. Comparisons between groups were made using 1-way ANOVA with Tukey's multiple-comparison test. *** $P < 0.001$ versus WT; \$\$\$ $P < 0.001$ versus *mdx^{4cv}* saline. μ Dys: micro-dystrophin, mDys and midi-Dys: midi-dystrophin, fDys and full-Dys: full-length dystrophin.

compared with WT (Figure 4C), while 39 upregulated and 7 downregulated proteins were found between full-Dys-*mdx*^{Acv} and WT mice (Figure 4D).

Further analysis of top upregulated and downregulated DEPs in *mdx*^{Acv} compared with WT gastrocnemius revealed that several cellular processes were dysregulated (Figure 5). For instance, upregulated DEPs in *mdx*^{Acv} muscle were enriched for molecular functions and biological processes, including protein and mRNA binding, cytoskeletal structure, supramolecular fiber organization, and regulation of RNA splicing, with cellular compartment enrichment for cytoplasmic, collagen-containing ECM, spliceosome, sarcolemmal, and endoplasmic reticulum proteins (Figure 5, A and B). Downregulated DEPs in *mdx*^{Acv} muscles, however, were enriched for molecular functions including nucleosomal DNA binding, fatty acid metabolic processes, and muscle tissue development, with the cellular compartment enrichment for DGC, sarcolemmal, cytoplasmic, and euchromatin-enriched proteins (Figure 5, A and C).

Importantly, several of these defects were partially restored with the dystrophin replacement using AAVMYO1 vectors at variable levels (Figures 5 and 6). For example, treatment with AAV- μ Dys5 restored the abundance of DGC proteins, including sarcoglycans (β , γ , and δ) and dystroglycans (Figure 3A, Figure 6, A and B, and Supplemental Figures 3 and 4), while the dual AAV-midi-Dys and triple AAV-full-Dys treatments resulted in similar patterns of proteomic restoration compared to *mdx*^{Acv} muscle but were slightly less effective in restoring sarcoglycan and dystroglycan levels (Figure 3A and Figure 6, A and B). In contrast, levels of α -syntrophin and utrophin were normalized with dual AAV-midi-Dys but remain slightly affected with μ Dys or triple AAV-full-Dys treatments (Figure 6, C and D, and Supplemental Figure 4), although utrophin levels were variable when assessed by Western blot (Supplemental Figure 4).

Similarly, several proteins with elevated abundance in WT muscle displayed reduced abundance in saline-treated *mdx*^{Acv}, whereas dystrophin construct expression mediated by AAV partially or fully restored their cellular enrichment, including protein-arginine deiminase type-2 and myoglobin (Figure 6E), as previously shown for myoglobin (26). In contrast, tubulin β 6 class V, whose abundance was higher in the saline group, consistent with a previous study (27), was greatly reduced in AAV-treated groups (Figure 6E).

In summary, these data confirm the depletion of the DGC in *mdx*^{Acv} muscle and corroborate other known disease sequelae in dystrophin-deficient muscle, including increased fibrosis and collagen deposition in the ECM, whereas μ Dys and intein-generated midi-Dys and full-Dys, respectively, restored 262, 258, and 235 out of 281 dysregulated proteins, which greatly improved the underlying cellular defects in *mdx*^{Acv} mice.

Dystrophin replacement partially restores biomarkers involved in membrane repair and myogenesis. Severe sarcolemmal fragility and susceptibility to cycles of damage and muscle regeneration represent a hallmark of DMD pathology due to the absence of dystrophin as a structural membrane protein. Disease-specific proteomic changes in *mdx* skeletal muscle include changes in cytoskeletal, structural, and membrane repair proteins (28). Based on our data demonstrating that more than 85% of *mdx*^{Acv} proteomic changes exhibit an intermediate or near-complete level of rescue by various-length AAV-Dys treatment, we investigated the impact of μ Dys5, midi-Dys, and full-Dys expression on membrane trafficking and repair proteins in *mdx*^{Acv} gastrocnemius muscle. A general trend of pathway elevation was observed in *mdx*^{Acv} muscle, with partial restoration across all AAV-Dys treatment groups (Figure 7A). Following this pattern, annexin A1 and annexin A5 levels were increased in *mdx*^{Acv} muscle compared with WT and partially restored by AAV-Dys treatment (Figure 7B). We also observed elevated annexin A4 levels in *mdx*^{Acv} muscle, but only AAV-midi-Dys treatment significantly reduced annexin A4 to an intermediate level between WT and dystrophin-deficient muscle (Figure 7B). Dysferlin also displayed elevated levels in saline-*mdx*^{Acv} muscles. While an intermediate restoration was detected in the AAV-treated groups, only dual midi-Dys treatment significantly reduced dysferlin levels compared to saline-*mdx*^{Acv} (Figure 7C and Supplemental Figure 4). Likewise, elevated levels of caveolin-3 and MG53/TRIM72 were found in control *mdx*^{Acv} muscle that were significantly but modestly reduced by AAV treatment (Figure 7C).

Furthermore, we analyzed the expression level of proteins implicated in membrane remodeling, trafficking, and cytoskeleton dynamics, such as clathrin light chain A, dynamin-2, and amphiphysin-2 (BIN1). These proteins were enriched in saline-*mdx*^{Acv} muscles, with 2- to 3-fold higher levels compared with WT muscles (Figure 7D). However, variable effects were found with the different dystrophin constructs. For instance, partial restoration was observed with the single AAV- μ Dys treatment, whereas near-complete normalization of these proteins was obtained with dual or triple AAV approaches (Figure 7D). Conversely, all dystrophin constructs restored the level of galectin-1 to WT levels and significantly reduced galectin-3, which were found to be 3- and 5-fold higher, respectively, in saline-treated dystrophic muscles (Figure 7, E and F).

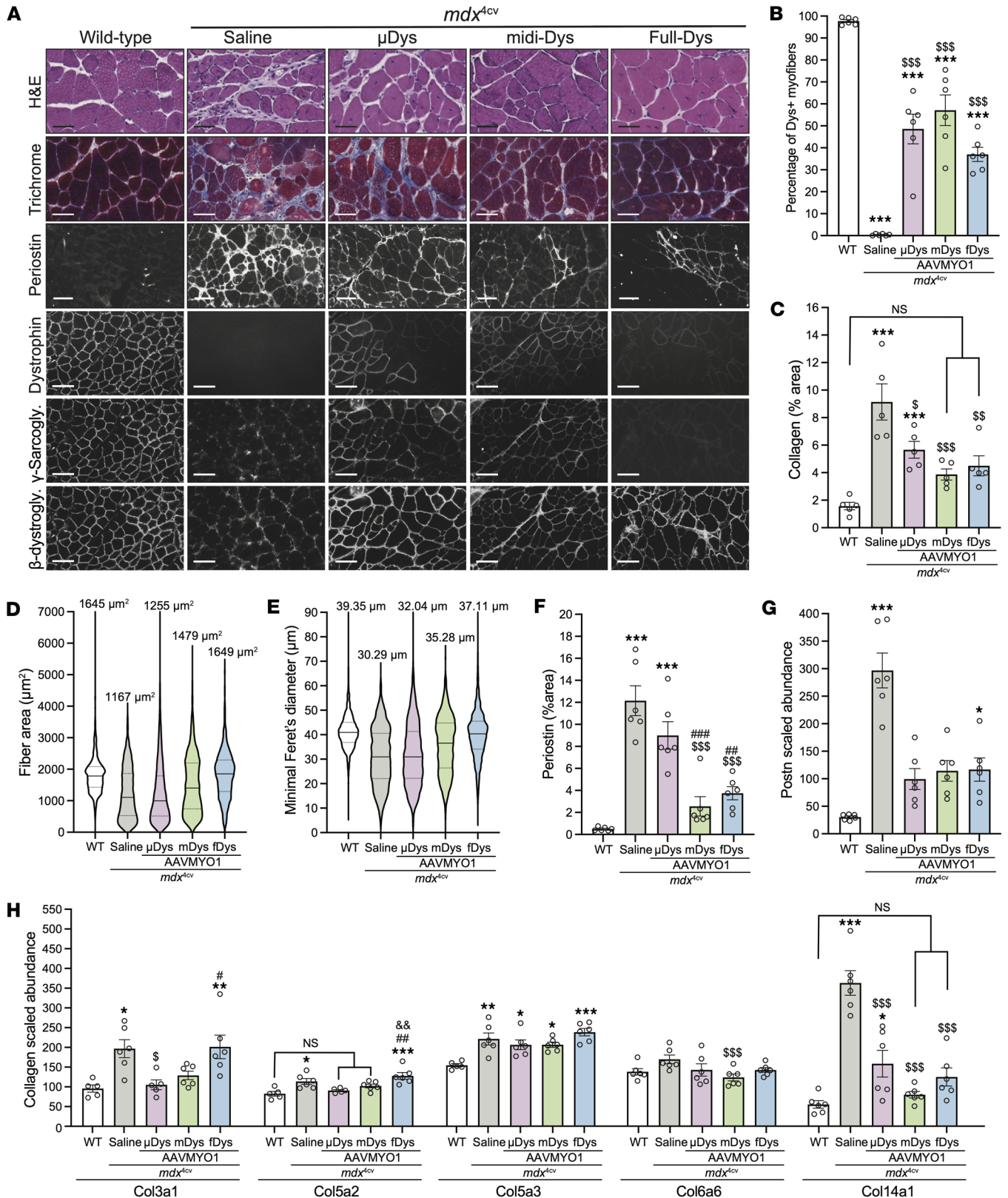


Figure 3. Histology analysis of gastrocnemius muscle cross sections showing improvements with dystrophin constructs. (A) Representative images of gastrocnemius muscle cross sections stained with H&E or trichrome (top rows, scale bars: 50 μm), or immunolabeled with antibodies specific for periostin (scale bars: 50 μm) or dystrophin-glycoprotein elements (lower panel, scale bars: 100 μm). These images were acquired in RGB colors but inverted to black and white for better visualization. The original panel is presented in Supplemental Figures 2 and 3. (B) Percentage of dystrophin-positive fibers; 600–1000 myofibers were counted per sample, with $n = 6$ analyzed per group. (C) The collagen area of the gastrocnemius muscle was measured using trichrome-stained cross sections. $n = 5$ samples per group. (D) Gastrocnemius myofiber area and (E) minimal Feret's diameter. More than 700 myofibers

per sample from $n = 6$ per group were analyzed. The average values are shown on top of the violin bars. The solid line represents the median, while the dashed lines show the quartiles. (F) Periostin area measured from cross-section muscle sections immunolabeled with specific antibodies against periostin. $n = 6$ samples per group. (G) Periostin abundance level detected from proteomics analysis of gastrocnemius muscles. (H) Abundance levels of different collagens were measured using the proteomics method from gastrocnemius samples. NS, not significant. $*P < 0.05$, $**P < 0.01$, $***P < 0.001$ versus WT; $^{\$}P < 0.05$, $^{\$\$}P < 0.01$, $^{\$ \$ \$}P < 0.001$ versus saline group; $^{\#}P < 0.05$, $^{\#\#}P < 0.01$, $^{\#\#\#}P < 0.001$ versus μ Dys group; $^{66}P < 0.01$ versus midi-Dys group using 1-way ANOVA followed by Tukey's post hoc test. Dys⁺: dystrophin-positive. H&E, hematoxylin and eosin; μ Dys, micro-dystrophin; mDys and midi-Dys, midi-dystrophin; fDys and full-Dys, full-length dystrophin.

These observations highlight the impairment of several key proteins involved in different pathways, including myogenesis, membrane repair, and remodeling in dystrophin-deficient myofibers, which were rescued to variable extents by dystrophin replacement strategies using single, dual, or triple AAVMYO1.

Incomplete corrections with dystrophin gene therapy. Based on the observation that mdx^{Acv} gastrocnemius muscles treated with single, dual, or triple AAV-Dys constructs retain some proteomic features that are distinct from healthy WT muscle (Figure 4), we sought to identify whether AAV-split-intein-Dys treatment results in unique, potentially pathological changes in protein expression and whether the unrestored DEPs in AAV-treated mdx^{Acv} muscle are relevant to DMD disease processes. We filtered our dataset for proteins that met the following 2 criteria: (a) significantly altered in AAV-treated mdx^{Acv} muscle compared with WT muscle, and (b) not significantly altered between AAV-treated and untreated mdx^{Acv} groups. After filtering, we obtained short lists of unrestored DEPs in μ Dys5- mdx^{Acv} , midi-Dys- mdx^{Acv} , and full-Dys- mdx^{Acv} gastrocnemius muscle (Figure 8, A–C). Several proteins demonstrated depleted abundance in mdx^{Acv} muscle that was not restored by the different dystrophin constructs, including carboxylesterase 1D (gene name *Ces1d*; Figure 8D), spermine oxidase (gene name *SmoX*; Figure 8E), tRNA methyltransferase 10 homolog C (gene name *Trmt10c*; Figure 8F), adenosylmethionine decarboxylase (gene name *Amd1*; Figure 8G), and histone H1.2 (gene name *H1-2*; Figure 8H). Levels of several upregulated proteins in mdx^{Acv} muscle were not ameliorated or were only partially ameliorated by AAV-dystrophin treatments, including myosin light chain 6B (gene name *Myl6b*; Figure 8I) and heme-binding protein 1 (gene name *Hebp1*; Figure 8J). Importantly, the introduction of split-intein dystrophin constructs did not induce unique or deleterious proteomic changes in the mdx^{Acv} gastrocnemius muscles. A singular protein, nicotinamide nucleotide transhydrogenase (NNT; gene name *Nnt*), demonstrated expression changes in mdx^{Acv} muscle that were more pronounced with AAV-dystrophin treatment; however, NNT expression levels did not display a statistically significant difference between treated and untreated mdx^{Acv} muscle (Figure 8K). Only 2 of the proteins identified as dysregulated in naive or AAV-treated mdx^{Acv} muscle, myosin light chain 4 (gene name *Myl4*) and hypoxanthine-guanine phosphoribosyltransferase (gene name *Hprt1*), were referenced in previous studies involving mdx mice (29–32). Notably, a singular protein, eukaryotic translation initiation factor 2D (gene name *Eif2d*), was identified as uniquely altered by AAV treatment (Figure 8L), suggesting a minimal biological impact of injection with the AAV constructs themselves.

Discussion

Genetic mutations in the *DMD* gene have been associated with the development of dystrophinopathies, a group of fatal diseases characterized by progressive degeneration of striated muscles. While the primary cause is the lack of functional dystrophin, leading to fragility of the sarcolemma membrane and high susceptibility to damage from muscle contraction, additional cellular defects are being revealed through studies involving patient-derived biological material or dystrophin-deficient cellular and animal models (33). A plethora of therapeutic strategies have emerged aiming to deliver or restore the expression of dystrophin or treat downstream disease sequelae by modulating several signaling pathways (34). However, measuring the effectiveness of these therapies was limited to the quantitation of dystrophin protein, the characterization of the general muscle histology, or measuring the mechanical properties of skeletal muscle. Here, we utilized a proteomics method to delineate a global protein expression profile in healthy or dystrophin-deficient murine muscles. Moreover, we used this method to validate the therapeutic outcomes of 3 different dystrophin replacement strategies in mdx^{Acv} mice and compiled a list of unrestored defects that might be used as biomarkers for future studies.

Our dataset confirms the depletion of DGC proteins and demonstrates an overall pattern of elevated expression for membrane trafficking and repair pathway proteins in mdx^{Acv} muscle, with partial restoration of some proteins by the different dystrophin constructs expressed via AAV delivery. Lower levels of DGC proteins were previously described in dystrophin-null muscles as a direct consequence of the absence of

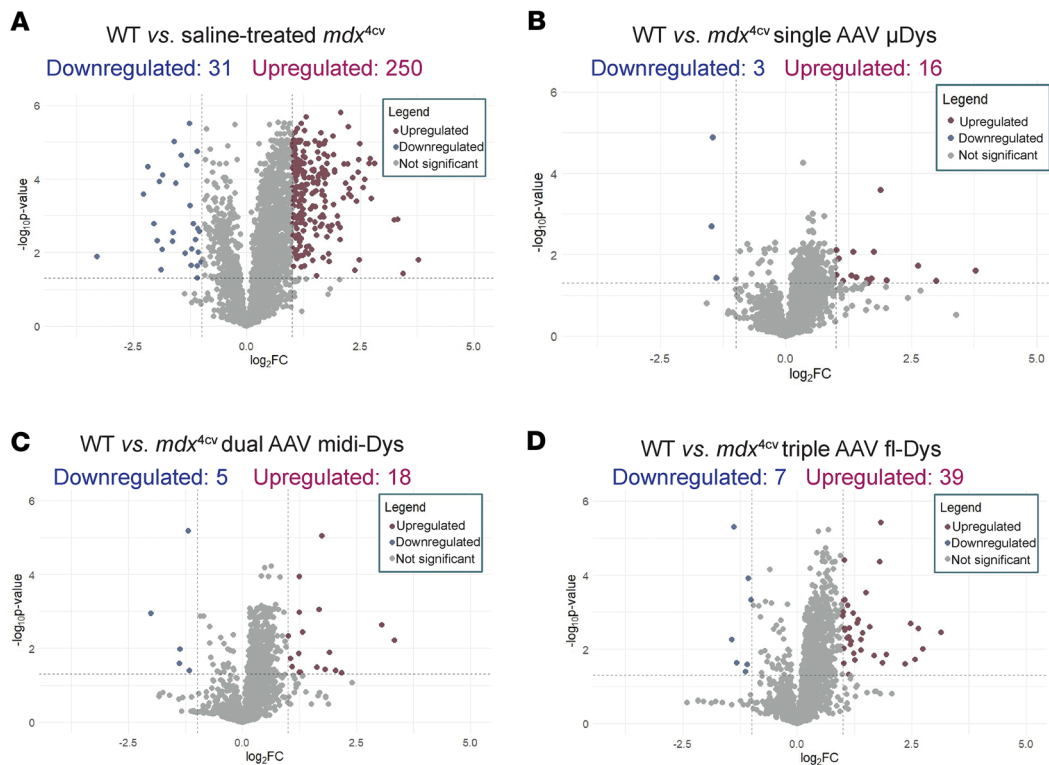


Figure 4. Comparison of protein expression profiles between experimental groups. Protein expression profiles in gastrocnemius muscle were compared between WT mice and (A) saline-*mdx*^{4cv}, (B) *mdx*^{4cv} injected with single AAVMYO1 μ Dys, (C) *mdx*^{4cv} injected with dual AAVMYO1 to express midi-dystrophin, or (D) *mdx*^{4cv} injected with triple AAVMYO1 vector to express full-length dystrophin. A 2-tailed, unpaired Student's *t* test was used to calculate *P* values for pairwise fold changes, and the Benjamini-Hochberg method was used to control the false discovery rate (FDR). Corrected *P* values were log-transformed and plotted against log-transformed fold change values to obtain volcano plots, and a minimum corrected *P*-value cutoff of 0.05 and minimum relative fold change cutoff of ± 1 were applied to identify differentially expressed proteins (DEPs) in pairwise comparisons. Data were collected from a sample size of $n = 6$ per group.

dystrophin (35, 36), whereas the upregulation of MG53/TRIM72, dysferlin, caveolin-3, utrophin, and members of the annexin family may reflect an adaptive response to increased sarcolemmal membrane fragility and rupture. The function of annexin A4 in sarcolemmal repair has not been clearly defined. However, overexpression of other annexin family members has been observed in DMD muscle as a response to increased membrane fragility and activation of membrane repair processes (37, 38). Interestingly, genetic mutations affecting the expression of dysferlin and caveolin-3 have been associated with the development of muscular dystrophies (39–42). In addition, several reports have shown the molecular interaction of MG53/TRIM72, dysferlin, and caveolin-3 in muscles and suggested their modulation as a potential therapeutic target in various muscular disorders (43–47).

Similarly, other proteins with essential roles in membrane trafficking and remodeling, including clathrin light chain 1, dynamin-2, and amphiphysin-2 (BIN1), were found expressed at high levels in dystrophin-null *mdx*^{4cv} muscles. These proteins were also linked to the pathogenesis of different congenital myopathies (48, 49). In the last decade, dynamin-2 and BIN1 have been extensively investigated as genetic modifiers in different muscular disorders (50–54), but their role in the pathogenesis of DMD has yet to be characterized. For instance, BIN1 and dynamin-2, as well as dysferlin and caveolin-3, are involved in transverse tubule (T-tubule) formation (55). These invaginations of the sarcoplasmic membrane associate with 2 sarcoplasmic reticula to form the triads, which are key regulators in excitation-contraction coupling. Early studies suggested the presence of dystrophin in the T-tubules (56, 57), while another study indicated structural and functional defects in the sarcoplasmic reticulum in dystrophin-deficient muscles, contributing to calcium homeostasis defects (58). Although the expression of dystrophin constructs with variable lengths using AAV vectors leads to changes in the expression profiles of the various proteins involved in membrane repair, trafficking, and remodeling, additional studies confirming the restoration of these cellular processes are needed.

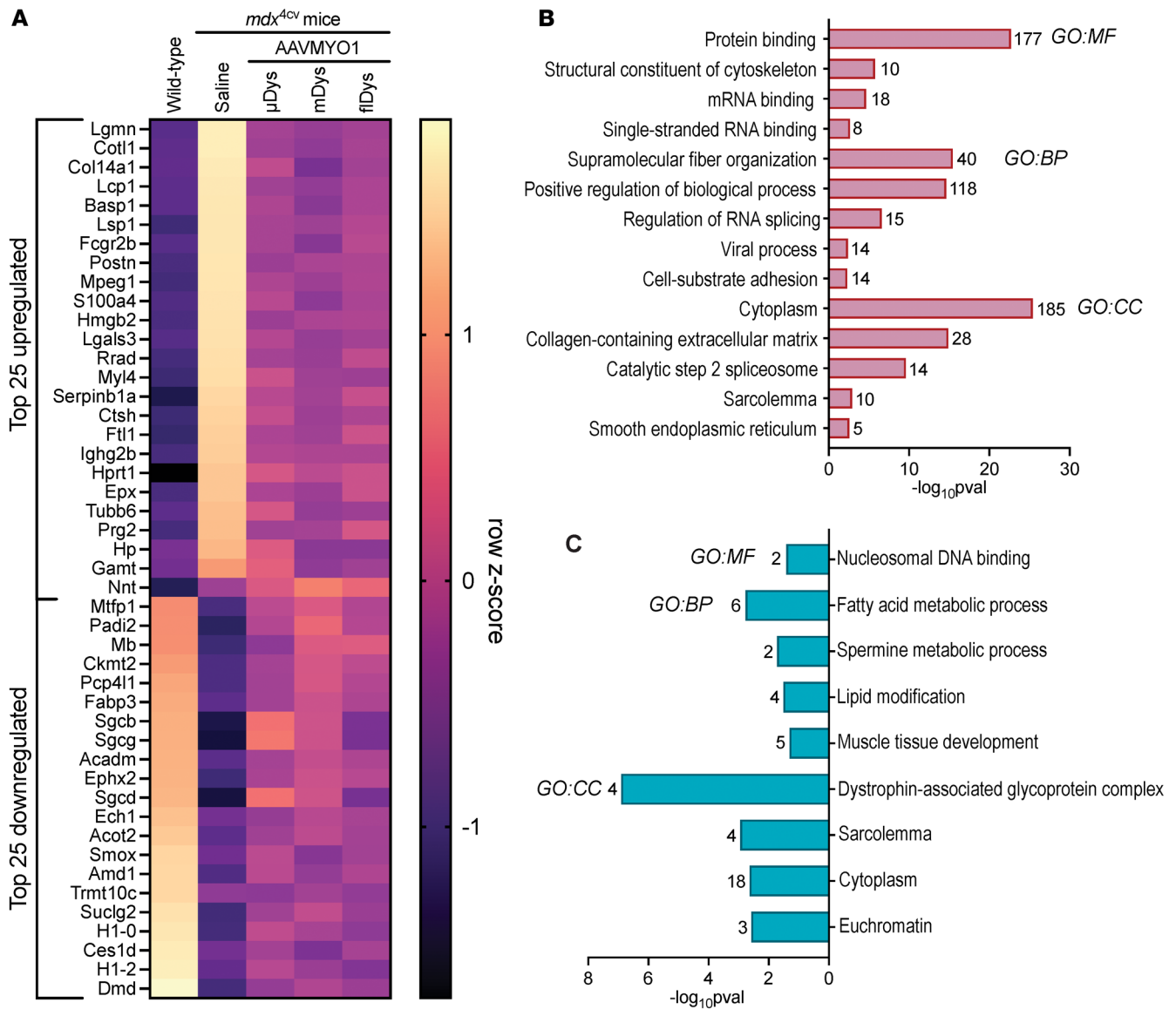


Figure 5. Analysis of protein expression profile demonstrates proteomic rescue by dystrophin constructs. (A) Heatmap depicting the top upregulated and downregulated proteins between WT and *mdx^{4cv}* muscle. Gene ontology (GO) enrichment analysis was performed using GOrilla and g:Profiler to determine the molecular function (MF), biological process (BP), and cellular compartment (CC) enrichment of significantly (B) upregulated and (C) downregulated proteins in *mdx^{4cv}* gastrocnemius muscle compared with WT muscle.

Our data confirm the upregulation of galectin-1 and galectin-3. Elevated levels of these proteins have been reported previously in cellular and animal models of DMD, as well as in patient-derived muscle samples (59–61). Recent work has linked galectin-3 to lysosomal damage in 2 mouse models of muscular dystrophy (61). In particular, AAV-mediated γ -sarcoglycan gene replacement normalized galectin-3 expression in the *Sgcb^{-/-}* mouse model of limb-girdle muscular dystrophy R5 (LGMDR5, γ -sarcoglycanopathy). In contrast, μ Dys supplementation in *mdx^{4cv}* mice resulted in limited rescue of lysosomal defects, which were hypothesized to arise from elevated galectin-3 levels (61). Our proteomic data demonstrate restoration of galectin-3 across all dystrophin constructs tested, including μ Dys. Differences in μ Dys sequence, expression cassette, AAV capsid (AAV9 versus the myotropic vector AAVMYO), and vector dose may underlie the divergent outcomes observed in *mdx^{4cv}* mice between the 2 studies. Nevertheless, our dataset lacks histopathological characterization of lysosomal damage-mediated defects. Further studies are warranted to elucidate the impact of these defects in skeletal muscle and to assess the therapeutic potential of different dystrophin constructs.

Additionally, using our proteomics approach, we correlated the increase in fibrosis found on muscle sections stained with trichrome to the upregulation of collagen XIV α 1, but not other collagen isoforms.

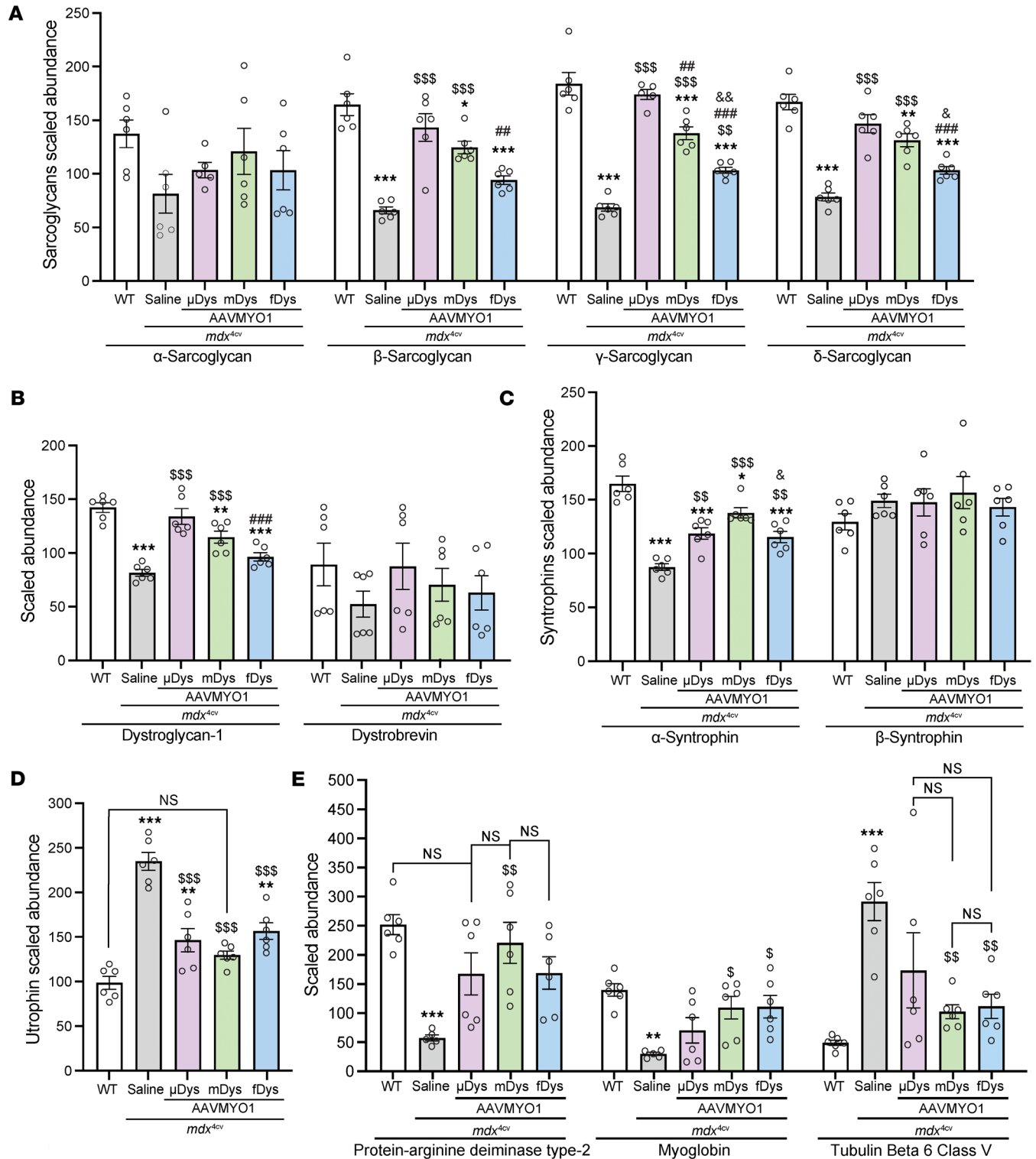


Figure 6. Dystrophin delivery alleviates DGC protein defects in *mdx^{4cv}* mice. Relative abundance of (A) sarcoglycans, (B) dystroglycan, dystrobrevin, (C) syntrophins, (D) utrophin, and (E) protein-arginine deiminase type-2, myoglobin, and tubulin β6 class V measured by the proteomics method. Bar graphs depict mean ± SEM from *n* = 5–6 mice/group. Comparisons between groups were made using 1-way ANOVA with Tukey’s multiple-comparisons test. NS, not significant. **P* < 0.05, ***P* < 0.01, ****P* < 0.001 versus WT; ⁵*P* < 0.05, ⁵⁵*P* < 0.01, ⁵⁵⁵*P* < 0.001 versus saline group; ###*P* < 0.01, ###*P* < 0.001 versus μDys group; ⁶*P* < 0.05, ⁶⁶*P* < 0.01 versus midi-Dys. μDys, micro-dystrophin; mDys, midi-dystrophin; fDys, full-length dystrophin.

Collagen XIVα1 plays a crucial role in the regulation of ECM organization and tissue integrity across various organs and has been linked to fibrotic disease as well as cardiovascular conditions (62). Nonetheless, most studies agree on the primary implication of collagen I (α1 and α2 chains) and collagen III in the

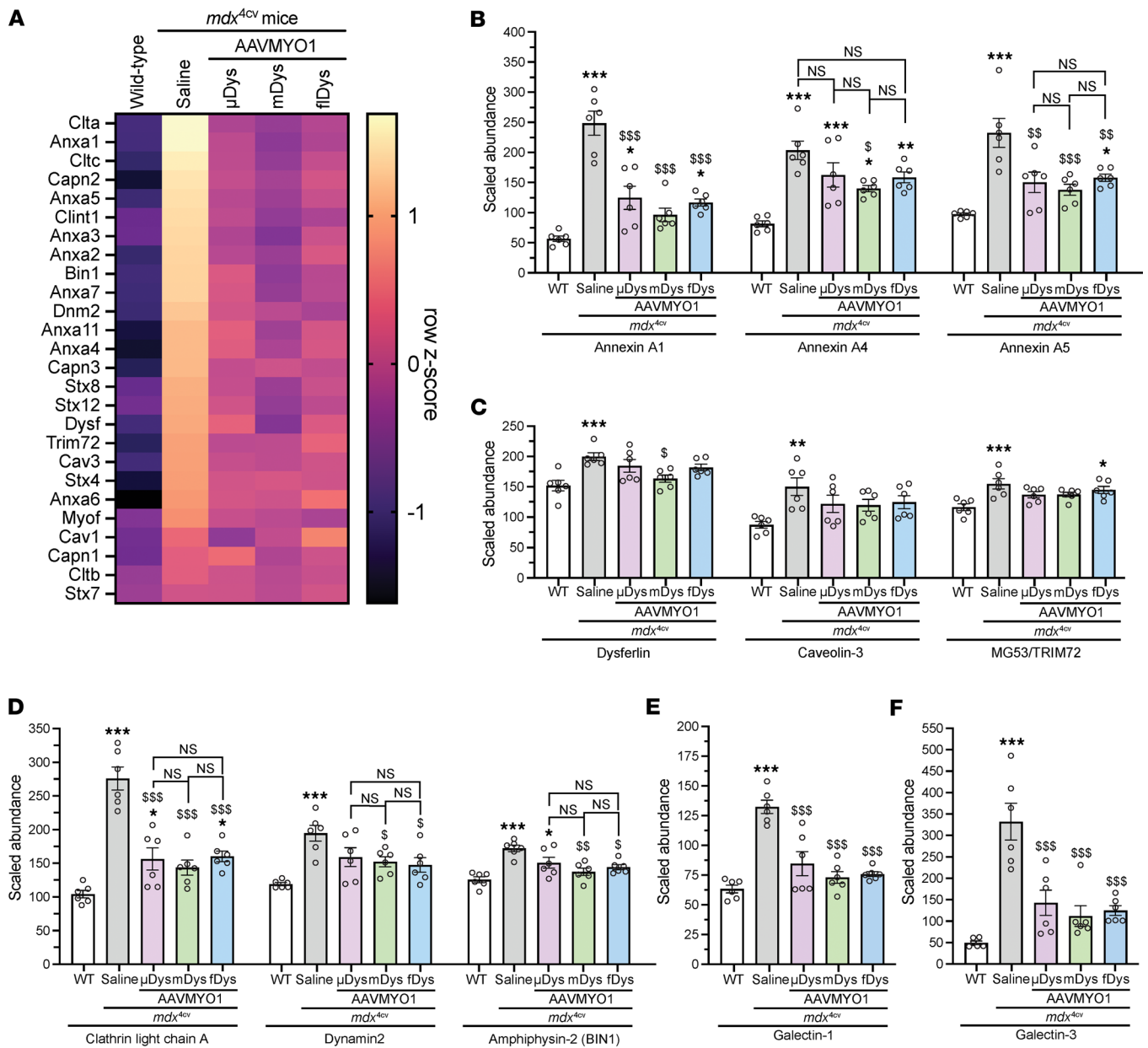


Figure 7. Amelioration of altered membrane repair and myogenesis pathway markers in *mdx^{4cv}* muscle mediated by AAV-dystrophin constructs. (A) Heatmap showing elevated expression of various proteins implicated in membrane trafficking and repair in *mdx^{4cv}* gastrocnemius muscle and partial restoration with μ Dys5, midi-dystrophin, or full-length dystrophin delivered by AAV vectors. **(B)** Annexin (A1, A4, and A5) abundance in WT, dystrophic, or AAV-treated muscles. **(C)** Abundance of proteins involved in muscle repair. **(D)** Expression of key proteins involved in membrane trafficking and remodeling. **(E)** Galectin-1 and **(F)** galectin-3 abundance in *mdx^{4cv}* and WT muscles. Bar graphs represent mean \pm SEM of $n = 6$ mice/group. NS, not significant. * $P < 0.05$, ** $P < 0.01$, *** $P < 0.001$ versus WT; $^{\$}P < 0.05$, $^{5\$}P < 0.01$, $^{55\$}P < 0.001$ versus saline group using 1-way ANOVA followed by Tukey's post hoc test. μ Dys, micro-dystrophin; mDys, midi-dystrophin; fDys, full-length dystrophin.

development of fibrosis in skeletal muscles (63–65). The time point chosen in this study (i.e., 5 months of age) is too premature to draw robust conclusions about the expression profile of the different collagen forms and their contributions to the mild and early-stage fibrosis found in the muscle sections. Moreover, our data confirmed the upregulation of periostin, which was previously identified as a profibrotic marker in *mdx* mice and other mouse models of muscular dystrophies (66, 67).

Furthermore, AAV-mediated delivery and expression of dystrophin constructs did not restore the expression profile of various proteins to WT levels. This could be explained by either the mosaic expression of dystrophin in only half of myofibers or the disease status and the age when AAVs were administered (8 weeks old and analysis 3 months after AAV infusion). At this age, *mdx* muscles may have already

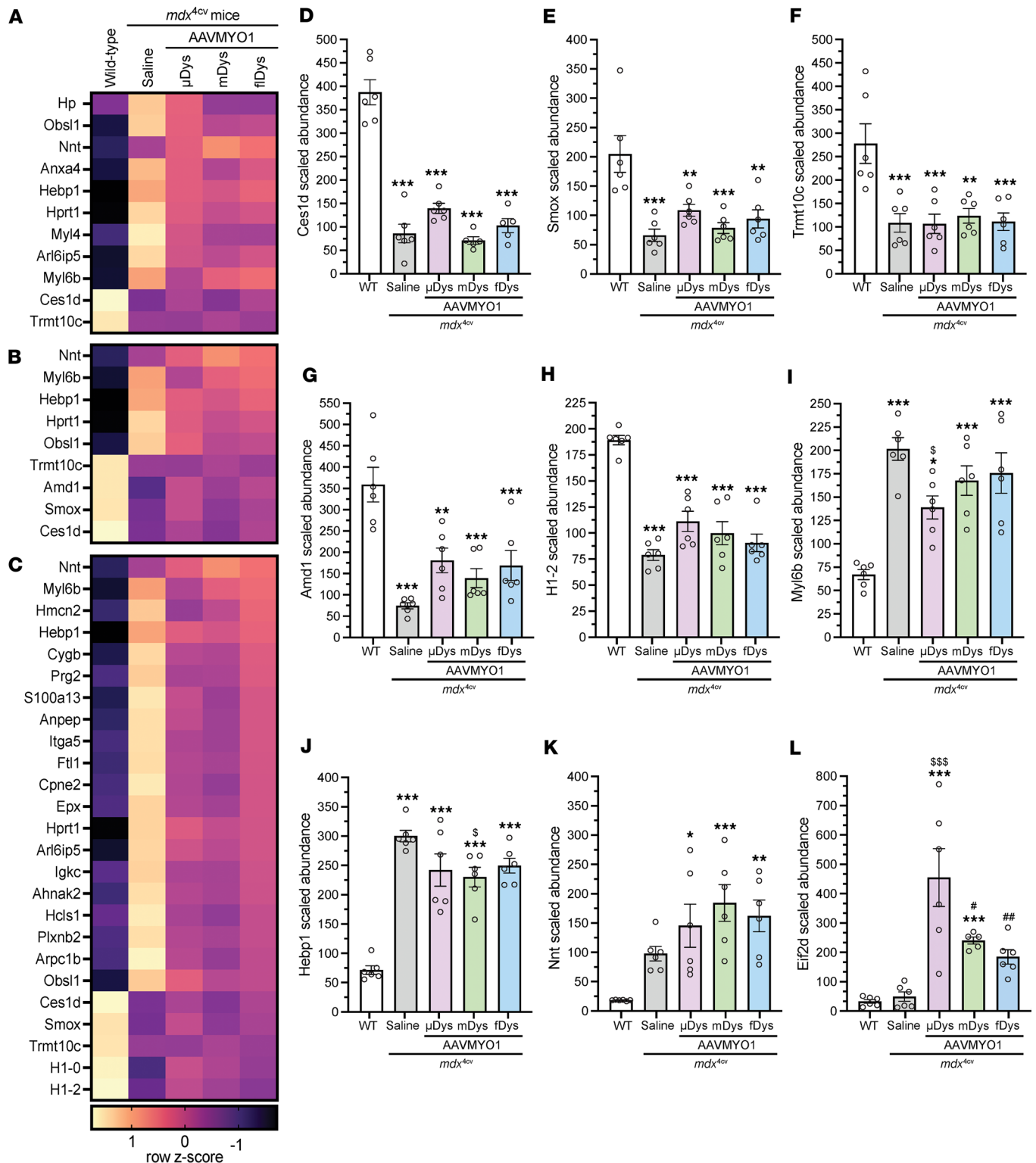


Figure 8. Proteins with unrestored expression in *mdx^{4cv}* mice treated with various dystrophin constructs. Heatmaps displaying proteins that did not display significant restoration to WT levels in (A) μ Dys5-*mdx^{4cv}*, (B) midi-Dys-*mdx^{4cv}*, or (C) full-Dys-*mdx^{4cv}* gastrocnemius muscles. Exemplary proteins with unrestored levels in AAV-Dys construct groups include (D) carboxylesterase 1D (Ces1d), (E) spermine oxidase (Smox), (F) tRNA methyltransferase 10 homolog C (Trmt10c), (G) adenosylmethionine decarboxylase (Amd1), (H) histone H1.2 (H1-2), (I) myosin light chain 6B (Myl6b), (J) heme-binding protein (Heb1), (K) nicotinamide nucleotide transhydrogenase (Nnt), and (L) eukaryotic translation initiation factor 2D (Eif2d). Bar graphs depict mean \pm SEM from $n = 5-6$ mice/group. Comparisons between groups were made using 1-way ANOVA with Tukey's multiple-comparison test. * $P < 0.05$, ** $P < 0.01$, *** $P < 0.001$ versus WT; § $P < 0.05$, \$\$\$ $P < 0.001$ versus saline; # $P < 0.05$, ## $P < 0.01$ versus μ Dys group. μ Dys, micro-dystrophin; mDys, midi-dystrophin; fDys, full-length dystrophin.

accumulated cellular, histological, and functional defects due to the absence of dystrophin during muscle development in the embryonic stage, as well as the postnatal phase (68, 69).

It is noteworthy that clinical trials of AAV- μ Dys also display mosaic expression of μ Dys and invariably enroll patients who have already begun developing dystrophic pathophysiology. At this stage, in both mice and patients, skeletal muscles have undergone many cycles of degeneration and regeneration crisis, and many, if not all, myofibers have been replaced (70). Previous studies have shown that the downregulation of genes encoding adenosylmethionine decarboxylase (*Amd1*) and spermine oxidase (*SmoX*) worsens the myopathy in the tibialis anterior muscle of mice with LAMA2-deficient congenital muscular dystrophy (71). More recent evidence suggests that dysregulated polyamine metabolism also contributes to muscle fiber defects in the context of amyotrophic lateral sclerosis (72). Increased urinary levels of spermine metabolites have been observed in patients with DMD for decades (73). However, there is not enough evidence available to support the central role of altered polyamine homeostasis in promoting skeletal muscle pathology in patients with DMD. The consequences of unrestored polyamine metabolic enzyme levels in *mdx*^{Acv} gastrocnemius muscle after AAV-dystrophin therapy are, therefore, unknown but unlikely to fully explain residual functional deficits in treated muscle.

In conclusion, this study describes the use of a proteomics approach to study the global protein expression in healthy or dystrophic skeletal muscles. This method can be implemented to validate therapeutic strategies in preclinical and clinical studies and monitor the effectiveness of treatments for muscular disease.

Methods

Sex as a biological variable. DMD is an X-linked disease affecting mainly boys. Therefore, only male *mdx* mice were used in this study. *mdx*^{Acv} female and male mice were used for breeding and generating mouse cohorts.

Animals. Mice were randomized into experimental groups based on availability. They were assigned a serial identification number to conduct a blinded study. These numbers were used throughout the study, and the treatment history of each mouse was determined after completing the data collection.

AAV production. μ Dys5 (Δ SR2–15, Δ SR18–21, Δ CT), split gp41.1/midi-Dys (Δ SR5–15) N- or C-terminal constructs, or split dystrophin with split Nrdj1 and split gp41.1 combination were inserted in pAAV containing the muscle-specific M-creatine kinase (CK) 8e expression cassette (CK8e, gift from Stephen D. Hauschka, University of Washington) and a synthetic polyA flanked by 2 inverted terminal repeats (17, 19). These constructs were packaged in the myotropic AAVMYO1 (gift from Dirk Grimm, University of Heidelberg) vectors using the conventional triple plasmid transfection of HEK293 cells as previously described (74).

AAV administration. Eight-week-old *mdx*^{Acv} males were anesthetized using isoflurane (Piramal Critical Care) before systemic administration of a low dose of AAVMYO1 into the tail vein (μ Dys: 2×10^{13} vg/kg, midi-Dys: 1×10^{13} vg/kg of each vector, full-Dys: 1.33×10^{13} vg/kg of each vector). As a control, a subgroup was injected with sterile saline. Once AAV or saline solutions were successfully administered, mice were kept in a warm cage and monitored for 1 hour.

Muscle histology analysis. Gastrocnemius muscles were isolated from 5-month-old WT or *mdx*^{Acv} mice and flash-frozen using liquid nitrogen-cooled isopentane. Cross-sections (10 μ m) were prepared using a cryostat (Leica CM1850) and stained with H&E or trichrome. Whole sections were imaged with the Hamamatsu NanoZoomer slide scanner, and the most representative sections are presented in this study. Other sections were immunolabeled overnight with antibodies against the dystrophin N-terminus (homemade, rabbit 246) (75), γ -sarcoglycan (NCL-g-SARC, Leica Biosystems), β -dystroglycan (NCL-b-DG, Leica Biosystems), periostin (ab1404150, Abcam), myosin heavy chains type I (BA-D5, DSHB), type IIa (SC-71, DSHB), type IIb (BF-F3, DSHB), or laminin 2 (L0663, rat, Sigma-Aldrich) diluted (1:100) in solutions containing Tris-buffered saline (TBS) with Tween 20 and 5% bovine serum albumin (BSA). Secondary antibodies goat anti-rabbit Alexa Fluor 790 (111-655-144, Jackson ImmunoResearch), goat anti-rabbit Alexa Fluor 488 (111-545-144, Jackson ImmunoResearch), goat anti-mouse IgG2a Alexa Fluor 488 (115-547-186, Jackson ImmunoResearch), goat anti-rabbit Alexa Fluor 594 mouse IgG2b (115-587-187, Jackson ImmunoResearch), goat anti-mouse IgG2b Alexa Fluor 350 (A21140, Invitrogen), goat anti-mouse IgM Alexa Fluor 488 (115-545-020, Jackson ImmunoResearch), goat anti-mouse IgG1 (115-587-185, Jackson ImmunoResearch), or goat anti-rat Alexa Fluor 594 (A11007, Invitrogen) were incubated for 2 hours diluted (1:100) in solutions containing TBS-Tween and 5% BSA. Slides were mounted using Immu-Mount (Epredia), and images were captured on a Nikon Eclipse 90i microscope. The myofiber size and minimal fiber diameter (miniFeret) were

determined from laminin-positive sections. The percentage of dystrophin-positive myofibers was quantified using sections stained with anti-dystrophin and -laminin antibodies, while dystrophin-positive fiber type percentage was quantified from sections quadruply stained for dystrophin and myosin heavy chains. The fibrosis area was measured using sections stained with trichrome. Periostin area was quantified from sections stained with anti-periostin antibodies. Fiji image analysis software (version 2.0.0-rc-68/1.52g) (76) was used to quantify all the histology parameters cited above.

Protein extraction, digestion, and peptide isobaric labeling. Frozen gastrocnemius muscle tissue pieces (20–25 mg) were processed using a Percellys Cryolys Evolution bead beater (Bertin Technologies). Tissue samples were weighed in Percellys tissue homogenizing CKMix tubes (Bertin Technologies) and protein extraction buffer (7 M urea, 2 M thiourea, 0.4 M Tris pH 8.0, 20% [v/v] acetonitrile, 10 mM Tris [2-carboxyethyl] phosphine [TCEP], 40 mM chloroacetamide, and 1 μ L/100 μ L buffer Pierce Universal Nuclease [Thermo Fisher Scientific]) was added at a ratio of 9 μ L lysis buffer per mg of tissue. A 150 μ L aliquot of each sample was transferred to a PCT tube with a 150 μ L cap for the Barocycler NEP2320 (Pressure Biosciences, Inc.) and cycled between 35 kPSI for 20 seconds and 0 kPSI for 10 seconds, for 60 cycles at 37°C. After barocycling, the samples were centrifuged at 15,000g for 10 minutes. The samples were transferred to new 1.5 mL microfuge Eppendorf Protein LoBind tubes. Aliquots for each sample were taken for protein concentration determination by Bradford assay.

A bridged pooled normalizing sample was made for 2 TMTpro 16plex (Tandem Mass Tag, Thermo Fisher Scientific) experiments. The pooled sample was composed of equal-microgram aliquots of each gastrocnemius sample. An 18 μ g aliquot of each sample and pooled sample was transferred to a new 1.5 mL Eppendorf Protein LoBind tube and brought to the same volume with extraction buffer. The samples were diluted 5-fold with LC-MS grade water. Next, trypsin (Promega) was added in a 1:40 ratio of trypsin to total protein. Samples were incubated at 37°C overnight, then were acidified with 0.3% (v/v) formic acid. Samples were cleaned using a MCX Stage tip (University of Minnesota Center for Metabolomics and Proteomics) and eluates were vacuum dried. Samples were resuspended with 0.1 M triethylammonium bicarbonate, pH 8.5, to a final protein concentration of 1 μ g/ μ L.

For stable isotope labeling, a 14 μ g aliquot for each sample was made and assigned a channel within a TMTpro 16plex. The samples were labeled with TMTpro 16plex isobaric label reagent in a 1:10 ratio of micrograms of protein to micrograms of TMTpro 16plex label according to the manufacturer's instructions. Isobaric tag-labeled samples within the same experimental screen were multiplexed together into a new 1.5 mL Eppendorf tube, then vacuum dried and cleaned with a 1 mL SepPak C18 solid phase extraction cartridge (Waters Corporation). Each TMTpro 16plex sample was vacuum dried, resuspended in 20 mM ammonium formate, pH 10, 98% (v/v) water and 2% (v/v) acetonitrile, and fractionated offline by high-pH C18 reversed-phase chromatography as previously described (77). After fractionation, concatenated peptide fractions were C18 Stage tipped (78) and eluates were dried in vacuo.

MS data acquisition. Skeletal muscle TMTpro 16plex proteomics experiments were performed at the University of Minnesota in collaboration with the Center for Metabolomics and Proteomics (CMSP) departmental core facility. Gastrocnemius muscle was extracted from 5 experimental groups of mice, including male WT (C57BL/6), untreated *mdx*^{Acv} (B6Ros.Cg-Dmd^{mdx-Acv}/J), μ Dys, midi-Dys, and full-Dys mice. Mice treated with low-dose AAV gene therapy constructs were sacrificed 3 months after treatment, and untreated WT and *mdx*^{Acv} mice were age matched with treated mice. Each group consisted of $n = 6$ biological replicates for a total of 30 samples. Two TMTpro 16plex screens were run sequentially to include all samples split equally between each screen, along with a pooled normalization control sample included in each screen. Peptide pellets were resuspended in solution consisting of 95% water, 5% acetonitrile, and 0.1% formic acid. The peptide mixture was vortexed for 45 seconds and centrifuged for 2 minutes at 4,000g. Data were collected on a Thermo Fisher Scientific Orbitrap Eclipse mass spectrometer coupled to a Dionex Ultimate 3000 RSLCnano LC pump. Peptides from 17% (2 μ L) of each concatenated set of fractions were separated using a 199-minute gradient at 0.315–0.325 μ L/min with a 0–90% Buffer B gradient at a column temperature of 55°C on a C18-AQ ReproSil-Pur column measuring 400 mm with an internal diameter of 100 μ m, 1.9 μ m resin size, and 120 Å pore size (Dr. Maisch GmbH Ammerbuch). Buffer A consisted of water with 0.1% (v/v) formic acid and Buffer B consisted of acetonitrile with 0.1% (v/v) formic acid. High-field asymmetric-waveform ion mobility spectroscopy (FAIMS) was enabled during experimental acquisition with the following compensation voltage (CV) settings: –45 V, –60 V, and –75 V. Voltage was kept at 2.1 kV for positive-ion mode and the ion transfer tube temperature was set to 275°C. At the MS1

stage, the mass spectrometer scanned masses in the range of 400–1400 m/z at a resolution of 120K with an AGC target of 4.0×10^5 over a 50-ms maximal injection time. At the MS2 stage, ions were fragmented by high-energy collisional dissociation (HCD) with a collision energy of 38% at a detector resolution of 50K with an AGC target of 1.25×10^5 (250% relative to default) over a 150-ms maximal injection time, and the Fourier transform first mass mode was fixed at 110 m/z .

Proteomics peptide spectrum matching and quantification. Raw MS files were processed by CMSP in Proteome Discoverer v3.1 (Thermo Fisher Scientific). Peptide identification was performed by searching HCD MS/MS files against the UniProtKB/Swiss-Prot *Mus musculus* database (UP000000589; accessed August 18, 2023) appended with custom dystrophin sequences from AAV-Myo1 μ Dys5, midi-Dys, and full-Dys constructs. Database search files were merged with a common lab contaminant database (<https://github.com/HaoGroup-ProtContLib>) with the Sequest HT search engine and a 1% false discovery rate (FDR) was set for peptide-to-spectrum matches using the Percolator algorithm in Proteome Discoverer v3.1. The following parameters were used for spectral processing: MS1 tolerance of 20 ppm, MS2 tolerance of 0.08 Da, trypsin (full) digestion with a maximum of 2 missed cleavages, minimum peptide length of 6 and maximum peptide length of 50, with 10 maximum peptides reported. Cysteine carbamidomethylation was set as a static modification, while TMTpro lysine and N-terminal modifications, asparagine and glutamine deamidation, methionine oxidation, pyro-glutamic acid, N-terminal acetylation, methionine loss, and methionine loss with acetylation were set as dynamic modifications in Sequest. Only protein identifications with high FDR confidence (FDR < 1%) and containing 2 or more peptides were accepted. Reporter ion quantification was conducted using the TMTpro 16plex (lot YD372049) quantification method with a peak integration tolerance of 20 ppm and the most confident centroid method. Unique and razor peptides were used for quantification. All peptides were used for normalization and protein roll-up, and scaling was performed for inter-screen data normalization using a pooled average control sample. Hypothesis testing was performed using a 2-tailed t test (background based) for pairwise ratios. Grubbs' test was used to identify and exclude single outlier data points.

Western blot. Proteins were extracted from gastrocnemius muscles using radioimmunoprecipitation analysis buffer (RIPA) supplemented with 1 mM PMSF and a 4% protease inhibitor cocktail (P8340, Sigma-Aldrich). Total protein concentration was determined using the Pierce BCA assay kit (Thermo Fisher Scientific). Samples were denatured at 100°C for 10 minutes, then 30 μ g of protein lysates were separated in NuPage 4%–12% Bis-Tris polyacrylamide gels (Invitrogen) using 165 V for 1 hour at room temperature. Protein transfer to 0.45 μ m PVDF membranes (Amersham Hybond) was performed at 120 V at 4°C for 2 hours. Membranes were blocked for 2 hours in TBS containing 5% nonfat dry milk and 0.005% Tween 20 before overnight incubation with antibodies against utrophin (from rabbit, gift from Froehner lab, University of Washington; ref. 79), dysferlin (Hamlet-CE, Leica Biosystems), γ -sarcoglycan (NCL-g-SARC, Leica Biosystems), or GAPDH (rabbit, G9545, Sigma-Aldrich) as a loading control. Secondary antibodies coupled to horseradish peroxidase were anti-mouse IgG2b (115-035-207, Jackson ImmunoResearch), anti-mouse IgG1 (115-035-205, Jackson ImmunoResearch), or goat anti-rabbit (111-035-144, Jackson ImmunoResearch). Blots were incubated for 2 hours at room temperature before visualization using Clarity Western ECL substrate (Bio-Rad) in the Chemidoc MP imaging system (Bio-Rad). The relative expression was determined by band densitometry measurements on unsaturated images using Fiji image analysis software.

Data availability. Source data to interpret, verify, and extend this research are provided in this paper. The MS proteomics data have been deposited to the ProteomeXchange Consortium via the PRIDE (80) partner repository with the dataset identifier PXD062324. Source data are provided in this paper. R script used to generate plots, filter, and analyze data is publicly available at: <https://github.com/joh18358/Split-in-tein-mdx-proteomics>. Values for all data points in graphs are reported in the Supporting Data Values file.

Statistics. Comparisons between all experimental groups were performed using 1-way ANOVA with Tukey's multiple-comparison correction. Scaled protein abundances were used to calculate pairwise fold changes based on the geometric means of all biological replicates from each sample group. Fold changes were calculated for pairwise comparisons between the following groups: mdx^{Acv}/WT , AAVMYO1 μ Dys5-treated mdx^{Acv}/WT , AAVMYO1 midi-Dys-treated mdx^{Acv}/WT , AAVMYO1 full-Dys-treated mdx^{Acv}/WT , mdx^{Acv}/μ Dys5-treated mdx^{Acv} , $mdx^{Acv}/$ midi-Dys-treated mdx^{Acv} , $mdx^{Acv}/$ full-Dys-treated mdx^{Acv} , μ Dys5-treated $mdx^{Acv}/$ midi-Dys-treated mdx^{Acv} , μ Dys5-treated $mdx^{Acv}/$ full-Dys-treated mdx^{Acv} , and

mid-Dys-treated mdx^{Acv} /full-Dys-treated mdx^{Acv} . A 2-tailed, unpaired Student's t test was used to calculate P values for pairwise fold changes, and the Benjamini-Hochberg method was used to control the FDR. Corrected P values were log-transformed and plotted against log-transformed fold change values to obtain volcano plots generated in R using the tidyverse package, and a minimum corrected P -value cutoff of 0.05 and minimum relative fold change cutoff of ± 1 was applied to identify DEPs in pairwise comparisons. Comparisons between all experimental groups were performed using 1-way ANOVA with Tukey's multiple-comparison correction. Full protein quantification datasets generated in Proteome Discoverer and lists of DEPs were imported to R for data filtering and visualization using the gplots, VennDiagram, and dplyr packages. Venn diagrams were used to obtain lists of overlapping and non-overlapping DEPs between distinct 2-group comparisons. Proteins with missing values for pooled samples in one or both screens were excluded from further analysis. Functional enrichment analysis was performed using Gorilla (81) and g:Profiler (82). For DEP gene ontology (GO) analysis, the target set included the DEP list and the background set the *Mus musculus* reference proteome. PCA plots were generated in R using the ggfortify package. One-way ANOVA statistical analysis and dataset filtering were performed in R. Bar graphs, GO enrichment visualizations, and heatmaps for DEPs of interest were performed in GraphPad Prism, version 10.2.

Study approval. All animal experiments were approved by the University of Washington's Institutional Animal Care and Use Committee (IACUC).

Author contributions

HT and JSC designed the AAV treatment and strategy. EEJ and JME conceptualized the proteomics study. HT produced and purified the AAV, injected mice, and collected muscle samples. EEJ prepared the muscle samples and proteins for proteomics analysis and performed the statistical and bioinformatic analysis. HT and TRR analyzed the muscle histology. HT and EEJ wrote the manuscript. JME and JSC provided reagents and edited the manuscript.

Funding support

This work is the result of NIH funding, in whole or in part, and is subject to the NIH Public Access Policy. Through acceptance of this federal funding, the NIH has been given a right to make the work publicly available in PubMed Central.

- Muscular Dystrophy Association grant 1060372.
- Association Française Contre Les Myopathies (AFM-Telethon, grant 24777).
- NIH grants P30 DK017047 and P50 AR065139 to the Diabetes Research Center and the Wellstone Center, respectively, at the University of Washington.
- US Department of Defense grant MD220097.
- Bettencourt-Schueller Foundation fellowship (to HT).
- Philippe Foundation fellowship (to HT).
- Association Française Contre Les Myopathies (AFM-Telethon) fellowship (to HT).
- NIH Minnesota Muscle Training Grant 5T32AR007612 (to EEJ).
- NIH grant 5R01AR042423 (to JME).
- NIH High-end Instrumentation Grant S10OD028717 (support for the Orbitrap Eclipse instrumentation platform used for proteomics data acquisition).

Acknowledgments

We thank the Viral Vector Core of the Sen. Paul D. Wellstone Muscular Dystrophy Specialized Research Center, the Histology and Imaging Core at the University of Washington, and the University of Minnesota Center for Metabolomics and Proteomics for the excellent technical assistance. We thank Dirk Grimm (University of Heidelberg) and Stephen D. Hauschka (University of Washington) for providing the AAVMYO1 and CK8e plasmids, respectively.

Address correspondence to: Hichem Tasfaout, Department of Neurology, University of Washington School of Medicine, Seattle, Washington, 98195, USA. Phone: 206.221.5412; Email: tasfaout@uw.edu.

1. Emery AE. The muscular dystrophies. *Lancet*. 2002;359(9307):687–695.
2. Ray PN, et al. Cloning of the breakpoint of an X;21 translocation associated with Duchenne muscular dystrophy. *Nature*. 1985;318(6047):672–675.
3. Monaco AP, et al. Detection of deletions spanning the Duchenne muscular dystrophy locus using a tightly linked DNA segment. *Nature*. 1985;316(6031):842–845.
4. Hoffman EP, et al. Dystrophin: the protein product of the Duchenne muscular dystrophy locus. *Cell*. 1987;51(6):919–928.
5. Ervasti JM, Campbell KP. Membrane organization of the dystrophin-glycoprotein complex. *Cell*. 1991;66(6):1121–1131.
6. Ervasti JM, Campbell KP. A role for the dystrophin-glycoprotein complex as a transmembrane linker between laminin and actin. *J Cell Biol*. 1993;122(4):809–823.
7. Bengtsson NE, et al. The road towards AAV-mediated gene therapy of Duchenne muscular dystrophy. *Mol Ther*. 2025;33(5):2035–2051.
8. Srivastava A, et al. Nucleotide sequence and organization of the adeno-associated virus 2 genome. *J Virol*. 1983;45(2):555–564.
9. England SB, et al. Very mild muscular dystrophy associated with the deletion of 46% of dystrophin. *Nature*. 1990;343(6254):180–182.
10. Harper SQ, et al. Modular flexibility of dystrophin: implications for gene therapy of Duchenne muscular dystrophy. *Nat Med*. 2002;8(3):253–261.
11. Davies KE, Vogt J. Long-term clinical follow-up of a family with Becker muscular dystrophy associated with a large deletion in the DMD gene. *Neuromuscul Disord*. 2024;39:5–9.
12. Phelps SF, et al. Expression of full-length and truncated dystrophin mini-genes in transgenic mdx mice. *Hum Mol Genet*. 1995;4(8):1251–1258.
13. Banks GB, et al. The polyproline site in hinge 2 influences the functional capacity of truncated dystrophins. *PLoS Genet*. 2010;6(5):e1000958.
14. Gregorevic P, et al. rAAV6-microdystrophin preserves muscle function and extends lifespan in severely dystrophic mice. *Nat Med*. 2006;12(7):787–789.
15. Ramos JN, et al. Development of novel micro-dystrophins with enhanced functionality. *Mol Ther*. 2019;27(3):623–635.
16. Birch SM, et al. Assessment of systemic AAV-microdystrophin gene therapy in the GRMD model of Duchenne muscular dystrophy. *Sci Transl Med*. 2023;15(677):eabo1815.
17. Tasfaout H, et al. Split intein-mediated protein trans-splicing to express large dystrophins. *Nature*. 2024;632(8023):192–200.
18. Shah NH, Muir TW. Inteins: nature's gift to protein chemists. *Chem Sci*. 2014;5(1):446–461.
19. Tasfaout H, et al. Expression of full-length dystrophin reverses muscular dystrophy defects in young and old mdx4cv mice. *J Clin Invest*. 2025;135(15):e189075.
20. Ibraghimov-Beskrovnaya O, et al. Primary structure of dystrophin-associated glycoproteins linking dystrophin to the extracellular matrix. *Nature*. 1992;355(6362):696–702.
21. McCourt JL, et al. Multi-omics analysis of sarcospan overexpression in mdx skeletal muscle reveals compensatory remodeling of cytoskeleton-matrix interactions that promote mechanotransduction pathways. *Skelet Muscle*. 2023;13(1):1.
22. Wang X, et al. Diverse effector and regulatory functions of fibro/adipogenic progenitors during skeletal muscle fibrosis in muscular dystrophy. *iScience*. 2023;26(1):105775.
23. Xin J, Liu S. Identifying hub genes and dysregulated pathways in Duchenne muscular dystrophy. *Int J Neurosci*. 2025;135(4):375–387.
24. Kalkan H, et al. Targeting gut dysbiosis against inflammation and impaired autophagy in Duchenne muscular dystrophy. *EMBO Mol Med*. 2023;15(3):e16225.
25. Tsonaka R, et al. Plasma lipidomic analysis shows a disease progression signature in mdx mice. *Sci Rep*. 2021;11(1):12993.
26. Olthoff JT, et al. Loss of peroxiredoxin-2 exacerbates eccentric contraction-induced force loss in dystrophin-deficient muscle. *Nat Commun*. 2018;9(1):5104.
27. Randazzo D, et al. Persistent upregulation of the β -tubulin tubb6, linked to muscle regeneration, is a source of microtubule disorganization in dystrophic muscle. *Hum Mol Genet*. 2019;28(7):1117–1135.
28. Rayavarapu S, et al. Identification of disease specific pathways using in vivo SILAC proteomics in dystrophin deficient mdx mouse. *Mol Cell Proteomics*. 2013;12(5):1061–1073.
29. Heezen LGM, et al. Spatial transcriptomics reveal markers of histopathological changes in Duchenne muscular dystrophy mouse models. *Nat Commun*. 2023;14(1):4909.
30. Boccanegra B, et al. Determination of qPCR reference genes suitable for normalizing gene expression in a novel model of Duchenne muscular dystrophy, the D2-mdx mouse. *PLoS One*. 2024;19(11):e0310714.
31. Hildyard JCW, et al. Identification of qPCR reference genes suitable for normalizing gene expression in the mdx mouse model of Duchenne muscular dystrophy. *PLoS One*. 2019;14(1):e0211384.
32. Hildyard JCW, et al. Determination of qPCR reference genes suitable for normalizing gene expression in a canine model of Duchenne muscular dystrophy. *J Neuromuscul Dis*. 2018;5(2):177–191.
33. Duan D, et al. Duchenne muscular dystrophy. *Nat Rev Dis Primers*. 2021;7(1):13.
34. Heydemann A, Siemionow M. A brief review of Duchenne muscular dystrophy treatment options, with an emphasis on two novel strategies. *Biomedicines*. 2023;11(3):830.
35. Li D, et al. Sub-physiological sarcoglycan expression contributes to compensatory muscle protection in mdx mice. *Hum Mol Genet*. 2009;18(7):1209–1220.
36. Hoyte K, et al. Transgenic overexpression of dystroglycan does not inhibit muscular dystrophy in mdx mice. *Am J Pathol*. 2004;164(2):711–718.
37. Croissant C, et al. Annexins and membrane repair dysfunctions in muscular dystrophies. *Int J Mol Sci*. 2021;22(10):5276.
38. Swaggart KA, et al. Annexin A6 modifies muscular dystrophy by mediating sarcolemmal repair. *Proc Natl Acad Sci U S A*. 2014;111(16):6004–6009.
39. Bashir R, et al. A gene related to *Caenorhabditis elegans* spermatogenesis factor fer-1 is mutated in limb-girdle muscular dystro-

- phy type 2B. *Nat Genet.* 1998;20(1):37–42.
40. Liu J, et al. Dysferlin, a novel skeletal muscle gene, is mutated in Miyoshi myopathy and limb girdle muscular dystrophy. *Nat Genet.* 1998;20(1):31–36.
41. Minetti C, et al. Mutations in the caveolin-3 gene cause autosomal dominant limb-girdle muscular dystrophy. *Nat Genet.* 1998;18(4):365–368.
42. Betz RC, et al. Mutations in CAV3 cause mechanical hyperirritability of skeletal muscle in rippling muscle disease. *Nat Genet.* 2001;28(3):218–219.
43. Cai C, et al. Membrane repair defects in muscular dystrophy are linked to altered interaction between MG53, caveolin-3, and dysferlin. *J Biol Chem.* 2009;284(23):15894–15902.
44. Weisleder N, et al. Recombinant MG53 protein modulates therapeutic cell membrane repair in treatment of muscular dystrophy. *Sci Transl Med.* 2012;4(139):139ra85.
45. He B, et al. Enhancing muscle membrane repair by gene delivery of MG53 ameliorates muscular dystrophy and heart failure in δ -sarcoglycan-deficient hamsters. *Mol Ther.* 2012;20(4):727–735.
46. Paleo BJ, et al. Reduced sarcolemmal membrane repair exacerbates striated muscle pathology in a mouse model of Duchenne muscular dystrophy. *Cells.* 2022;11(9):1417.
47. Han R, et al. Dystrophin deficiency exacerbates skeletal muscle pathology in dysferlin-null mice. *Skelet Muscle.* 2011;1(1):35.
48. Nicot AS, et al. Mutations in amphiphysin 2 (BIN1) disrupt interaction with dynamin 2 and cause autosomal recessive centronuclear myopathy. *Nat Genet.* 2007;39(9):1134–1139.
49. Bitoun M, et al. Mutations in dynamin 2 cause dominant centronuclear myopathy. *Nat Genet.* 2005;37(11):1207–1209.
50. Lionello VM, et al. BIN1 modulation in vivo rescues dynamin-related myopathy. *Proc Natl Acad Sci U S A.* 2022;119(9):e2109576119.
51. Cowling BS, et al. Reducing dynamin 2 expression rescues X-linked centronuclear myopathy. *J Clin Invest.* 2014;124(3):1350–1363.
52. Tasfaout H, et al. Antisense oligonucleotide-mediated Dnm2 knockdown prevents and reverts myotubular myopathy in mice. *Nat Commun.* 2017;8:15661.
53. Cowling BS, et al. Amphiphysin (BIN1) negatively regulates dynamin 2 for normal muscle maturation. *J Clin Invest.* 2017;127(12):4477–4487.
54. Fugier C, et al. Misregulated alternative splicing of BIN1 is associated with T tubule alterations and muscle weakness in myotonic dystrophy. *Nat Med.* 2011;17(6):720–725.
55. Al-Qusairi L, Laporte J. T-tubule biogenesis and triad formation in skeletal muscle and implication in human diseases. *Skelet Muscle.* 2011;1(1):26.
56. Watkins SC, et al. Immunoelectron microscopic localization of dystrophin in myofibres. *Nature.* 1988;333(6176):863–866.
57. Hoffman EP, et al. Subcellular fractionation of dystrophin to the triads of skeletal muscle. *Nature.* 1987;330(6150):754–758.
58. Bellinger AM, et al. Hypernitrosylated ryanodine receptor calcium release channels are leaky in dystrophic muscle. *Nat Med.* 2009;15(3):325–330.
59. Cerri DG, et al. Degeneration of dystrophic or injured skeletal muscles induces high expression of galectin-1. *Glycobiology.* 2008;18(11):842–850.
60. Marotta M, et al. Muscle genome-wide expression profiling during disease evolution in mdx mice. *Physiol Genomics.* 2009;37(2):119–132.
61. Jaber A, et al. Lysosomal damage is a therapeutic target in Duchenne muscular dystrophy. *Sci Adv.* 2025;11(43):eadv6805.
62. Tao G, et al. Collagen XIV is important for growth and structural integrity of the myocardium. *J Mol Cell Cardiol.* 2012;53(5):626–638.
63. Foidart M, et al. Collagen localization in normal and fibrotic human skeletal muscle. *Arch Neurol.* 1981;38(3):152–157.
64. Alexakis C, et al. Implication of the satellite cell in dystrophic muscle fibrosis: a self-perpetuating mechanism of collagen overproduction. *Am J Physiol Cell Physiol.* 2007;293(2):C661–C669.
65. Duance VC, et al. The location of three collagen types in skeletal muscle. *FEBS Lett.* 1977;79(2):248–252.
66. Lorts A, et al. Deletion of periostin reduces muscular dystrophy and fibrosis in mice by modulating the transforming growth factor-beta pathway. *Proc Natl Acad Sci U S A.* 2012;109(27):10978–10983.
67. Trundle J, et al. Expression of the pro-fibrotic marker periostin in a mouse model of Duchenne muscular dystrophy. *Biomedicines.* 2024;12(1):216.
68. Merrick D, et al. Muscular dystrophy begins early in embryonic development deriving from stem cell loss and disrupted skeletal muscle formation. *Dis Model Mech.* 2009;2(7-8):374–388.
69. Granet JA, et al. Muscle stem cells in Duchenne muscular dystrophy exhibit molecular impairments and altered cell fate trajectories impacting regenerative capacity. *Cell Death Dis.* 2025;16(1):437.
70. DiMario JX, et al. Fiber regeneration is not persistent in dystrophic (MDX) mouse skeletal muscle. *Dev Biol.* 1991;148(1):314–321.
71. Kemaladewi DU, et al. Increased polyamines as protective disease modifiers in congenital muscular dystrophy. *Hum Mol Genet.* 2018;27(11):1905–1912.
72. Ruggieri V, et al. Polyamine metabolism dysregulation contributes to muscle fiber vulnerability in ALS. *Cell Rep.* 2025;44(1):115123.
73. Russell DH, Stern LZ. Altered polyamine excretion in Duchenne muscular dystrophy. *Neurology.* 1981;31(1):80–83.
74. Halbert CL, et al. AAV6 vector production and purification for muscle gene therapy. *Methods Mol Biol.* 2018;1687:257–266.
75. Rafael JA, et al. Forced expression of dystrophin deletion constructs reveals structure-function correlations. *J Cell Biol.* 1996;134(1):93–102.
76. Rasband, W.S., ImageJ, U. S. National Institutes of Health, Bethesda, Maryland, USA, <https://imagej.net/ij/>, 1997–2018.
77. Chaanine AH, et al. Multi-omics approach profiling metabolic remodeling in early systolic dysfunction and in overt systolic heart failure. *Int J Mol Sci.* 2021;23(1):235.
78. Rappsilber J, et al. Stop and go extraction tips for matrix-assisted laser desorption/ionization, nanoelectrospray, and LC/MS sample pretreatment in proteomics. *Anal Chem.* 2003;75(3):663–670.

79. Kramarcy NR, et al. Association of utrophin and multiple dystrophin short forms with the mammalian M(r) 58,000 dystrophin-associated protein (syntrophin). *J Biol Chem.* 1994;269(4):2870–2876.
80. Perez-Riverol Y, et al. The PRIDE database at 20 years: 2025 update. *Nucleic Acids Res.* 2025;53(d1):D543–D553.
81. Eden E, et al. GOrilla: a tool for discovery and visualization of enriched GO terms in ranked gene lists. *BMC Bioinformatics.* 2009;10:48.
82. Raudvere U, et al. g:Profiler: a web server for functional enrichment analysis and conversions of gene lists (2019 update). *Nucleic Acids Res.* 2019;47(w1):W191–W198.